Available online at www.sciencedirect.com
ScienceDirect
Journal of Power Sources 175 (2008) 33–39
JOURNAL OF POWER SOURCES
www.elsevier.com/locate/jpowsour

Behaviors and mechanism of electrolyte electrophoresis during electrophoretic deposition

Sian-Jie Ciou [a], Kuan-Zong Fung [a], Kai-Wei Chiang [b,*]

[a] *Department of Materials Science and Engineering, National Cheng Kung University, Tainan 70101, Taiwan*
[b] *Department of Geomatics, National Cheng Kung University, Tainan 70101, Taiwan*

Received 11 July 2007; received in revised form 26 September 2007; accepted 26 September 2007
Available online 2 October 2007

Abstract

Electrochemical experiments, including cyclic voltammetry (CV) experiments, galvanostatic experiments, potentiostatic experiments, and kinetic experiments of the LSM electrode, were used to investigate the influence of a deposit on the electrode surface on the electrophoresis of protons in a porous media during electrophoretic deposition (EPD).

In the kinetic experiments, the deposit reduced the electrochemical reaction rate of the LSM electrode according to the Tafel plots for the cathode where the YSZ was deposited. It was also observed that hydrogen was reduced at the cathode from the cyclic voltammogram. In the galvanostatic experiments, the proton concentration increased near the cathode because the deposit obstructed the electrode reaction. In the potentiostatic experiments, similar phenomena were observed. The deposit from the EPD became an obstacle to the electrochemical reaction, resulting in unusual kinetic behaviors of proton electrophoresis during electrolysis.

Keywords: Electrophoretic deposition; Electrophoresis; Finite element method

Electrophoretic deposition (EPD) is a two-step process. First, the charged colloidal particles in the suspension migrate to one of the electrodes under an external electric field [1,2]. EPD relies on the ability of the colloidal particles to obtain an electric charge in the solution where they are dispersed. In general, when solid powders such as a metal oxide are dispersed in a solution, the surfaces of the oxide interact with the liquid through simple ionization reactions of surface groups:

$$S - O^- \overset{OH^-}{\longleftrightarrow} S - OH \overset{H^+}{\longleftrightarrow} S - OH^+ \quad (1)$$

The second deposition step involves a complex combination of electrochemical and aggregation phenomena. The electric current is generated in two ways: the releasing of surface ions of colloidal particles, such as the protons on the oxide surface, and the free ions in suspension [3]. If the moving colloidal oxide particles and the free protons in the solution attach to the electrodes, it results in the re-dox reaction:

$$2H^+ + 2e^- \overset{\text{reduction}}{\longrightarrow} H_2 \overset{\text{oxidation}}{\longrightarrow} 2H^+ + 2e^- \quad (2)$$

Although several efforts have been made to study this process, it is not fully understood how to control the formation of an EPD because of the many parameters that must be considered and the fact that the mechanism itself has not been studied in detail. Hamaker [1], Hamaker and Verwey [2], and Koelmans and Overbeek [4] proposed that the applied external electric field controls the particles in suspension and the adhesion of the particles to the electrode is governed by the accumulation of products on the electrode surface. Sarkar and Nicholson [5] proposed that the aggregation and deposition of charged particles during EPD results from lyosphere distortion and thinning. However, few studies have focused on the relationship between electrolyte electrophoresis and the deposition mechanism during EPD [6]. Therefore, the primary objective of this experiment was to discover the behavior of electrolyte electrophoresis among the porous deposited layer during EPD using a potentiostat/galvanstat. The concentration profiles near the electrodes were simulated by a

* Corresponding author. Tel.: +886 6 2757575x63829.
E-mail address: kwchiang@mail.ncku.edu.tw (K.-W. Chiang).

0378-7753/$ – see front matter © 2007 Elsevier B.V. All rights reserved.
doi:10.1016/j.jpowsour.2007.09.077

Nomenclature

A	area of the electrode
C_j^*	the initial concentration of species j
D_j	diffusion coefficient of species j
e	electron charge
F	Faraday's constant
G	the body force term
I	the electric current through the cell
J_j	flux of species j
k	Boltzmann constant
K	permeability of the porous structure
n	the numbers of the species j
p	pressure
t	time
T	temperature
z_j	the valance of species j

Greek symbols

α	transfer coefficient
ζ_p	zeta potential of YSZ colloidal particles
η	the dynamic viscosity
κ	conductivity
μ	convection velocity
μ_j	mobility of species j
ρ	density of the fluid
τ	transition time
Φ	electric potential
Φ^Θ	equilibrium potential
Ω	domain
$\partial\Omega$	boundary

finite-element method to investigate the causes of the phenomena.

1. Theoretical background

The assumption used in the present study is that the kinetic behavior of electrophoresis in porous media is the same as general electrophoresis. In this sense, for a constant current, Sand's equation can be used to describe the kinetic behavior of electrolyte electrophoresis [7]:

$$\frac{i\tau^{1/2}}{C_j^*} = \frac{nFAD_j^{1/2}\pi^{1/2}}{2} \tag{3}$$

where τ is the transition time when the electrolyte concentration becomes zero on the electrode surface, D_j is the diffusion coefficient of species j, A is the area of the electrode, C_j^* is the initial concentration of species j, n is the numbers of species j, i is the electric current through the cell, and F is Faraday's constant. Here, the electrochemical reaction can be considered a non-reversible reaction; therefore, the electric potential is linearly dependent $\ln(\tau^{1/2} - t^{1/2})$ if the rate-determining step is a diffusion-controlled reaction, where t represents time.

In the potentiostatic experiments, the kinetic behaviors of corresponding current obey the Cottrell equation because EPD is assumed to be a diffusion-controlled reaction [6]:

$$i = \frac{nFAD_j^{1/2}C_j^*}{\pi^{1/2}t^{1/2}} \tag{4}$$

This implies that the current is linearly dependent on $t^{-1/2}$ if the rate-determining step is diffusion controlled, similar to the conclusions drawn for constant current.

2. Experimental procedure

2.1. Preparation of the $LaSrMnO_3$ substrate

The precursor $LaSrMnO_3$ (LSM) powders were prepared by La_2O_3 (Alfa), MnO_2 (Aldrich), and $Sr(NO_3)_2$ (Aldrich). The stoichiometrical amount of these precursors was mixed with ethanol (99.8% Kanto Chemicals, Tokyo, Japan). Afterward, the powders were milled, sieved, and then calcined at 1200 °C. The calcined powders were pressed into a disk, and sintered at 1400 °C. The diameter of the LSM-disk after heat treatment was about 10 mm.

2.2. Suspension for EPD

Yttria-stabilized zirconia (YSZ) suspension (TZ-8Y, Tosho) was prepared in solvents of ethanol (99.8%, Kanto Chemicals, Tokyo, Japan). The powder was dispersed in the suspension using an ultrasonic horn (DC400H, Delta) for 30 min. The pH (TDK-5721S) value was adjusted to 4.03 using acetic acid (Fluka).

2.3. The apparatus and geometry of EPD

The three-probe electrochemical cell was used in this study. The working electrode was the prepared LSM disk; the reference electrode was Ag/Ag^+ because ethanol was used as a solvent. In the experiments, the potential difference between the working and reference electrodes was controlled for the galvanstat or measured for the potentiostat. The counter electrode was a carbon electrode with a large surface area of 36 cm^2, so the Helmholtz capacitance of the counter electrode was negligible in this analysis.

2.4. Electrochemical experiments

In the study, the electrochemical experiments, which included cyclic voltammetry (CV) experiments, galvanostatic experiments, potentiostatic experiments, and the kinetic experiments of the LSM electrode, were conducted using an EG&G Model 273 potentiostat/galvanostat. In the CV experiments, the potential applied to the electrode was swept between −2.0 and 2.0 V (Ag/Ag^+). The scan rates used were 75 mV s^{-1}. The current that passed through the cell was measured during the potential scan.

In the galvanostatic experiments, a constant current ranging from −2 to −100 μA cm^{-2} was applied to the cell and the

potential of the working electrode was measured as a function of time.

In the potentiostatic experiments, a constant potential ranging from −1.5 to −5 V was applied on the working electrode to excite an electrochemical reaction. The current passing through the electrochemical cell was measured for 700 s.

In the experiments on the kinetics of the LSM electrode, the Tafel plot was used to illustrate the kinetic parameters of the LSM electrode where the YSZ accumulated on the surface to investigate the influence of the deposit on proton electrophoresis.

3. Results and discussions

3.1. Kinetics and the electrochemical reaction of the LSM electrode

Fig. 1 shows the Tafel plots of the LSM electrode, which was the cathode in the cell, in the prepared suspension and the blank solution. The blank solution was the same composition as the suspension without the YSZ powders. The interception for the suspension was −4.17 μA, and it decreased to −10.47 μA for the blank solution. This reduction of equilibrium current implied that the deposited YSZ layer would obstruct the electrochemical reaction of the LSM electrode.

The cyclic voltammogram for pH 4.03 YSZ suspension is given in Fig. 2. Oxygen evolution at the anode began at 0.4 V. This is considered the general re-dox potential of oxygen. The increase in the current at −0.8 V was most likely due to the proton reduction at the cathode. The relevant electrochemical reaction under the experimental conditions present in the EPD cell was the oxygen evolution at the anode:

$$H_2O \rightarrow 2H^+ + 1/2\,O_2 + 2e^- \quad (5)$$

The water present may have been from the residual water in ethanol or the producing water of esterification (acetic acid + ethanol).

At the cathode, the electrochemical reaction relevant to the particle deposition under the experimental conditions was

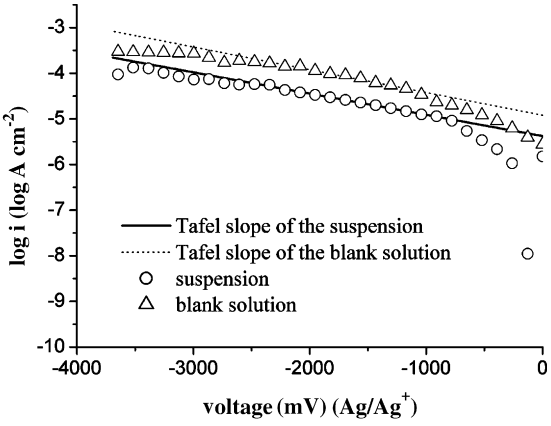

Fig. 1. The Tafel plots for the LSM cathode in the prepared suspension and blank solution. The interceptions are −10.47 μA for the blank solution and −4.17 μA for the suspension.

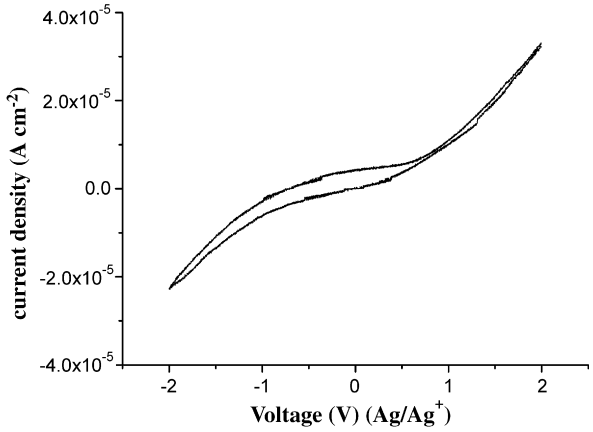

Fig. 2. The cyclic voltammogram for an LSM electrode with scanning rate of 75 mV s^{-1}. The current increase at 0.4 V is for oxygen evolution and −0.8 V for hydrogen evolution.

hydrogen reduction:

$$2H^+ + 2e^- \rightarrow H_2 \quad (6)$$

3.2. Constant current

Based on Sand's equation, the chronopotentiometry data for cathodic current of the YSZ suspension of −2 and −6 μA cm^{-2} versus $\ln(\tau^{1/2} - t^{1/2})$ is shown in Fig. 3, where the values of τ were 1482.59 s for −2 μA and 164.73 s for −6 μA. It was observed that there were linear regions for the initial 12 s when EPD was conducted at −2 μA and 5 s for EPD at −6 μA. These values indicate that the proton concentration was reduced from the initial concentration during the specific periods and that the rate-determining step was diffusion controlled. As time passed, the influence of the deposited YSZ layer became more significant on the reaction rate. The rate-determining step transformed into reaction-rate-controlled when the reaction rate decreased to a certain level. And the proton concentration even increased to larger than the initial concentration. To prove this hypothesis, a profile of proton concentration was simulated to try to explain how this phenomenon occurred. The finite element method [8–12] using the MATLAB 7.0 pdetool box was used for this calculation. The geometric calculations, including the domain and boundaries, are given in the Fig. 4. The cathode was 1 μm in diameter, and the pre-deposited layer from the sedimentation was 100 nm thick. The distance between the cathode and anode was approximately 10 μm. The symbols Ω_{dep} and Ω_{sus} represent the domain of the deposited layer and the suspension for the governing equations. The deposited layer was a porous structure formed by deposited YSZ particles.

3.2.1. Governing equations

Because the current was attributed to the flux of ionic species in the suspension, $CH3COO^-$ (called Ac^- in the present research), the free protons not adsorbed on the YSZ surface, the charged colloidal particles consisting of YSZ, and adsorbed ionic species were taken into account. The thickness of the

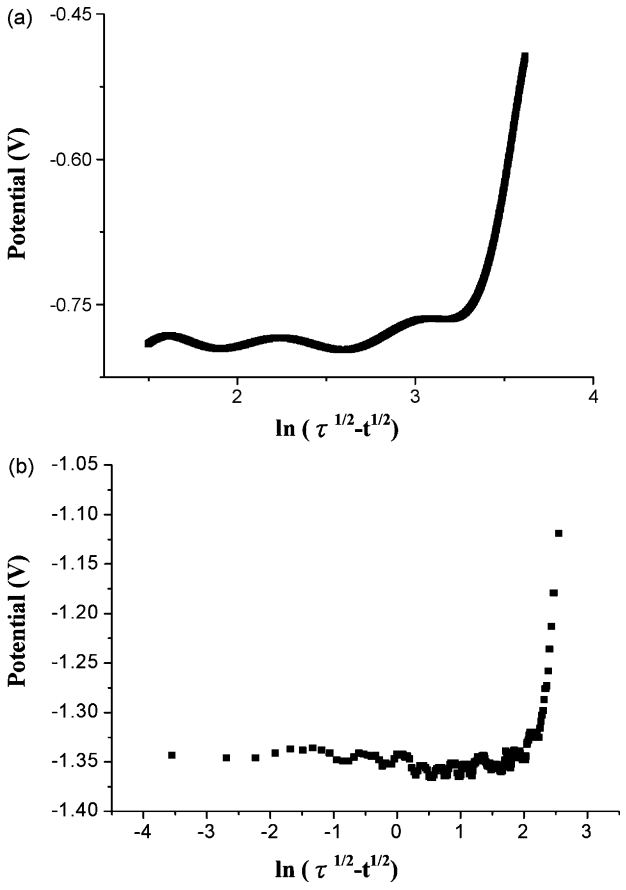

Fig. 3. The variation of electrical potential versus the $\ln(\tau^{1/2} - t^{1/2})$ for applied current density (a) −2 μA and (b) −6 μA.

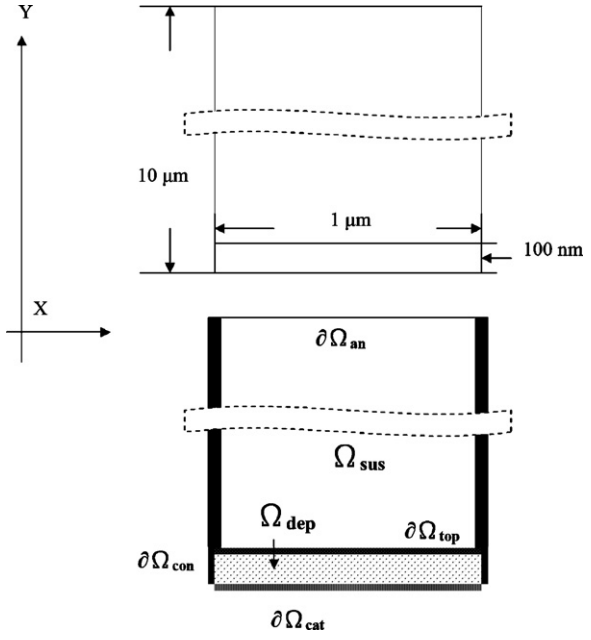

Fig. 4. 2D Schematic drawing of the deposited layer geometry for model. Here, Ω_{sus} represents the domain for the suspension, Ω_{dep} represents the domain for the deposit layer, $\partial\Omega_{cat}$ represents the boundary for the cathode, $\partial\Omega_{an}$ represents the boundary for the anode, $\partial\Omega_{top}$ represents the boundary for the top of the deposit, and $\partial\Omega_{con}$ represents the wall of the container.

deposit was too small to be significant. Mass balance, momentum balance, and energy conservation were applied to describe the profile of the YSZ concentration in the cell during EPD.

3.2.2. Mass balance

The Nernst–Plank equation that describes the conservation of ion species in suspension is:

$$\frac{\partial C_j}{\partial t} + \nabla(-D_j\nabla C_j - z_j\mu_j F C_j \nabla\Phi) = 0 \tag{7}$$

where C_j represents the concentration of species, j the protons H, Ac^-, YSZ, etc; and D_j is the diffusivity of species j in ethanol. For YSZ colloidal particles, z_j is the valance of each species, D_{YSZ} is obtained from the calculation of the Hűckel equation: $D_{YSZ} = \zeta_p/1.5\eta$ where ζ_p is the zeta potential of YSZ colloidal particles, and η is the viscosity of the suspension.

For YSZ colloidal particles, the valance values represent the number of charges the colloidal particles carry. In addition, the values of z_{YSZ} can be calculated from the zeta potential of YSZ colloidal particles where μ_j is the mobility of species j, F is Faraday's constant, Φ is the applied electric potential, and μ is the convection velocity. The initial value of μ is zero because the electrophoretic deposition began without stirring.

3.2.3. Momentum balance

Because the deposit layer was a porous media, the Brinkman equation was used to describe the flow in which momentum transports by shear stress. It can be written as:

$$\rho\frac{\partial u}{\partial t} - \nabla(\nabla u + (\nabla u)^{\mathrm{T}}) + \left(\frac{\eta}{K} + \nabla p - G\right) = 0$$
$$\nabla u = 0 \tag{8}$$

where η denotes the dynamic viscosity, ρ is the density of the fluid, p is the pressure, and K is the permeability of the porous structure. The G term is the body force term, which includes the influence of Brownian motion and the electric field, defined as:

$$G = kT\nabla C_j + eZ_jC_j\nabla\Phi \tag{9}$$

where T is the temperature.

3.2.4. Energy conservation

The current density is given by Faraday's law as:

$$i = -F\sum z_j^2\mu_j F C_j\nabla\Phi \tag{10}$$

Eq. (10) can be Ohm's law for ionic current transport and can be simplified as:

$$i = -\kappa\nabla\Phi \tag{11}$$

where κ is the conductivity of the electrolyte. A current balance gives the current and potential density in the cell as:

$$\nabla i = \nabla(-\kappa\nabla\Phi) = 0 \tag{12}$$

where the κ is the function of proton concentration:

$$\kappa = F\sum_i |z_i|\mu_i C_i \tag{13}$$

3.2.5. Boundary conditions and initial condition

The boundary for the anode, $\partial\Omega_{an}$, takes the form:

$$\begin{aligned}&\text{mass balance}: J_H = -J_H^0; J_{YSZ} = -f(C_{YSZ}, t);\\ &\quad C_{Ac-} = C_{Ac-}(t)\\ &\text{momentum balance}: u = 0\\ &\text{energy balance}: -ni = -i_0\end{aligned} \tag{14}$$

The boundary for cathode, $\partial\Omega_{cat}$, takes the form:

$$\begin{aligned}&\text{mass balance}: J_H = J_H^0; C_{YSZ} = \text{constant};\\ &\quad C_{Ac-} = C_{Ac-}(t)\text{momentum balance}: p \rightarrow \text{constant}\\ &\text{energy balance}: ni = i_0\end{aligned} \tag{15}$$

Here, the concentration of YSZ is constant because the YSZ particles are deposited on the cathode surface, and it is assumed that no additional YSZ particles are compressed into the deposited layer.

The boundary for the two sides of container, $\partial\Omega_{con}$, takes the form:

$$\begin{aligned}&\text{mass balance}: nJ_H = 0\\ &\text{momentum balance}: nu = 0\\ &\text{energy balance}: ni = 0\end{aligned} \tag{16}$$

Eventually, because the top of the deposit layer, $\partial\Omega_{top}$, was an inner boundary, the boundary conditions were continuous. The initial conditions are listed in Table 1.

3.2.6. Simulation Results

The calculations for proton concentration variation during EPD at constant −2 and −6 μA for 3, 6, 9, and 12 s are shown in Fig. 5. This is the electrolyte concentration profile along the bisector of the deposit. Because the protons were the charge carriers, the variation in the proton concentration was interesting. The horizontal axis represents the thickness of the deposit

Table 1
A summary of each parameter for galvanostatic simulation

Description	Notation	Unit	Value
Diffusion coefficient of proton	D_H	$m^2\,s^{-1}$	9.31×10^{-9}
Diffusion coefficient of Ac^-	D_{Ac-}	$m^2\,s^{-1}$	1.23×10^{-9}
Diffusion coefficient of YSZ	D_{YSZ}	$m^2\,s^{-1}$	5.31×10^{-9}
Mobility of a proton in ethanol	μ_H	$m^2\,J^{-1}\,s^{-1}$	3.78×10^{-12}
Mobility of Ac^- in ethanol	μ_{Ac-}	$m^2\,J^{-1}\,s^{-1}$	4.84×10^{-13}
Mobility of YSZ in ethanol	μ_{YSZ}	$m^2\,J^{-1}\,s^{-1}$	2.14×10^{-12}
Initial concentration of protons	C_H^*	M	9.33×10^{-5}
Initial concentration of YSZ	C_{Ac-}^*	M	9.33×10^{-5}
Initial concentration of YSZ	C_{YSZ}^*	M	3.96×10^{-9}
Initial convection velocity	μ_0	$m\,s^{-1}$	0
Initial pressure	P_0	Pa	0
Viscosity of ethanol	η	Pa s	1.074×10^{-3}
Density of ethanol	ρ	$kg\,m^{-3}$	790
Valance charge of a proton	z_H	NaN	1
Valance charge of Ac^-	z_{Ac-}	NaN	−1
Valance charge of YSZ	z_{YSZ}	NaN	50
Initial conductivity of suspension	κ_0	$S\,m^{-1}$	3.3×10^{-4}
Initial flux of proton	J_H^0	$mol\,m^{-2}\,s^{-1}$	1.04×10^{-5}
Initial Current density	I_0	$A\,m^{-2}$	−0.02, −0.06
Permeability of deposit	K	m^2	1×10^{-15}

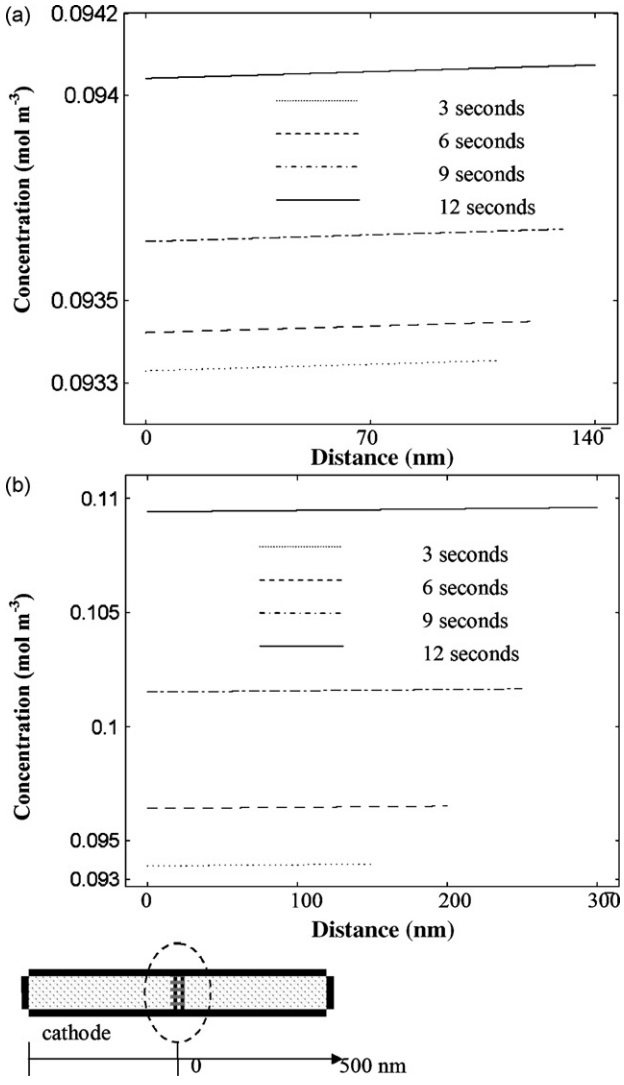

Fig. 5. The yields of simulation for proton concentration variation along the marked line during EPD at constant current of (a) −2 μA and (b) −6 μA for different time periods. The initial proton concentration is 0.0933 ($mol\,m^{-3}$).

layer. Based on Fig. 5(a), the proton concentration near the cathode was higher than the initial value, 0.0933 ($mol\,m^{-3}$), and the thickness grew from 100 nm to 110 nm after EPD for 3 s at −2 μA. A similar tendency can be seen at 6, 9, 12 s at −2 μA. Thus, the proton concentration increased as time passed, and the final proton concentration exceeded the initial proton concentration. As for EPD at −6 μA, Fig. 5(b), the proton concentration increased more dramatically. It was assumed that the proton concentration near the cathode would be much lower than the bulk concentration, and be reduced from the initial value because of hydrogen reduction. However, the proton concentrations increased, even exceeding the initial proton concentration. Based on the Tafel plot, the deposit layer would obstruct the electrode reaction rate, so this unusual accumulation of the proton concentration can be attributed to the obstruction of the deposit layer. Thus, the porous deposit layer blocked the path of transportation of the electrolyte, and reduced the active site on the electrode surface. This resulted

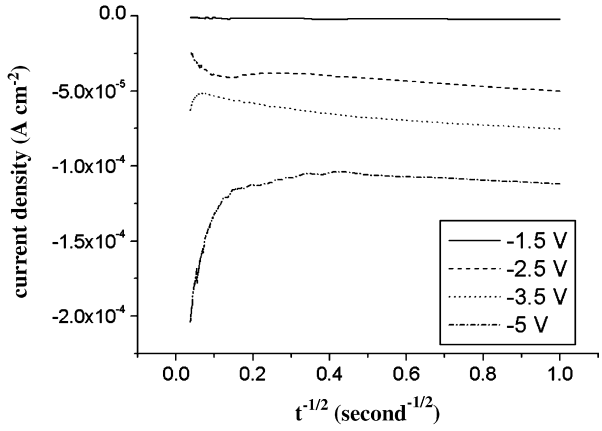

Fig. 6. The data for current density versus $t^{-1/2}$ during potentostatic EPD at different applied voltages for 700 s.

in the reaction rate being smaller than the diffusion velocity, so the whole reaction was reaction-rate controlled. It was completely different from the tendency of general galvanostatic experiments, in which the electrolyte concentration would be consumed during the electrochemical reaction, reaching zero near the electrode.

3.3. Constant voltage

The way the current varied with $t^{-1/2}$ during EPD at different constant voltages is shown in Fig. 6. Initially, there were linear regions in every curve, as illustrated in the first 10 s for −2.5 V. This transformed to a non-linear relationship after this critical point. As the current was increased, the critical time period occurred earlier, i.e., 2 s for −5 V. The expected tendency was linear, implying the rate-determining step was the diffusion velocity of the proton through the deposit. However, as time passed, the influence of the deposit on the reaction rate resulted in the accumulation of protons near the electrode, and the kinetic behaviors departing from Cottrell's prediction. To prove this hypothesis, the proton concentration variation during EPD at constant voltage was simulated, similar to the constant current simulation. Two voltages, −2.5 and −12.5 V, were used as the source from the external electrical field. In this simulation, the assumptions, geometries, and governing equations were the same as those for a constant current.

3.3.1. Boundary conditions and initial condition

The boundary of the top of the anode, $\partial\Omega_{an}$, takes the form:

$$\begin{aligned}&\text{mass balance}: j_H = -J_H^0\left\{\frac{C_H}{C_H^*}\exp\left[-\alpha\frac{F}{RT}(\Phi-\Phi^{\Theta})\right]\right\};\\ &J_{YSZ} = -f(C_{YSZ}, i); C_{Ac-} = C_{Ac-}(t)\\ &\text{momentum balance}: p \rightarrow \text{constant}\\ &\text{energy balance}: \Phi = f(y)\end{aligned} \quad (17)$$

Here, the electric potential is a function of position because the thickness of the deposited layer increased with time.

The boundary for anode, $\partial\Omega_{cat}$, takes the form:

$$\begin{aligned}&\text{mass balance}: J_H = J_H^0\left\{\frac{C_H}{C_H^*}\exp\left[-\alpha\frac{F}{RT}(\Phi-\Phi^{\Theta})\right]\right\};\\ &C_{YSZ} = \text{constant}; C_{Ac-} = C_{Ac-}(t)\\ &\text{momentum balance}: u = 0\\ &\text{energy balance}: \Phi = 0\end{aligned} \quad (18)$$

The boundary for the two sides of container, $\partial\Omega_{con}$, takes the form:

$$\begin{aligned}&\text{mass balance}: nj_H = 0\\ &\text{momentum balance}: nu = 0\\ &\text{energy balance}: \Phi = \text{constant}\end{aligned} \quad (19)$$

Eventually, because the top of the deposit layer, $\partial\Omega_{top}$, was an inner boundary, the boundary conditions became continuous.

The initial conditions are listed in Table 2

3.3.2. Simulation results

The simulation results for EPD at constant voltages of −2.5 and −12.5 V for 5, 10, 15, and 20 s are shown in Fig. 7. As with the results for constant current, the protons accumulated near the cathode and increased as time passed. These variations yielded the same conclusion that the deposited layer obstructed the reaction rate and transferred the reaction from a diffusion-controlled reaction to a reaction-rate-controlled reaction. Interestingly, the concentration gradient was reversed when EPD was performed at −12.5 V for 20 s, as shown in Fig. 7(b). This phenomenon can be explained by the contribution of the high electrical force due to the diffusion of the electrolytic ions. Such a high electric voltage certainly resulted in the fast diffusion velocity, and the difference between the amounts of the proton consumption at the cathode and the amounts of the proton arrivals at the cathode was large enough to result in this interesting phenomenon.

Table 2
A summary of each parameter for potentiostatic simulation

Description	Notation	Unit	Value
Diffusion coefficient of proton	D_H	$m^2\ s^{-1}$	9.31×10^{-9}
Diffusion coefficient of Ac^-	D_{Ac-}	$m^2\ s^{-1}$	1.23×10^{-9}
Diffusion coefficient of YSZ	D_{YSZ}	$m^2\ s^{-1}$	5.31×10^{-9}
Mobility of a proton in ethanol	μ_H	$m^2\ J^{-1}\ s^{-1}$	3.78×10^{-12}
Mobility of Ac^- in ethanol	μ_{Ac-}	$m^2\ J^{-1}\ s^{-1}$	4.84×10^{-13}
Mobility of YSZ in ethanol	μ_{YSZ}	$m^2\ J^{-1}\ s^{-1}$	2.14×10^{-12}
Initial concentration of protons	C_H^*	M	9.33×10^{-5}
Initial concentration of YSZ	C_{Ac-}^*	M	9.33×10^{-5}
Initial concentration of YSZ	C_{YSZ}^*	M	3.96×10^{-9}
Initial convection velocity	μ_0	$m\ s^{-1}$	0
Initial pressure	P_0	Pa	0
Viscosity of ethanol	η	Pa s	1.074×10^{-3}
Density of ethanol	ρ	$kg\ m^{-3}$	790
Valance charge of a proton	z_H	NaN	1
Valance charge of Ac^-	z_{Ac-}	NaN	−1
Valance charge of YSZ	z_{YSZ}	NaN	50
Initial conductivity of suspension	κ_0	$S\ m^{-1}$	3.3×10^{-4}
Permeability of deposit	K	m^2	1×10^{-15}
Transfer coefficient	α	NaN	0.028
Initial applied potential	Φ_0	V	−12.5, −2.5
Equilibrium potential	Φ^{Θ}	V	−0.8

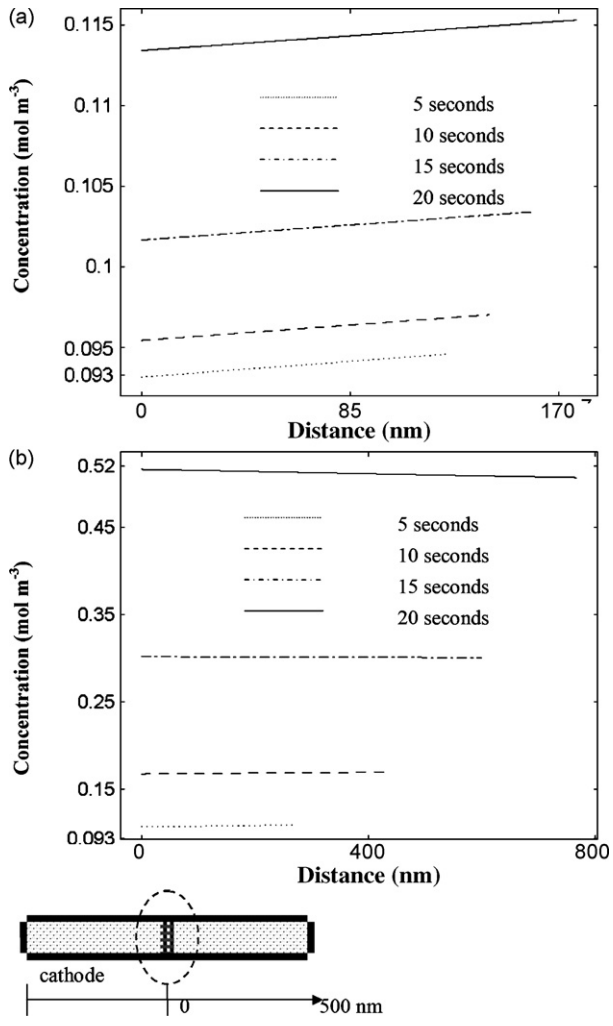

Fig. 7. The yields of simulation for proton concentration variation along the marked line during EPD at constant current of (a) −2.5 V and (b) −12.5 V for different time periods. The initial proton concentration is 0.0933 (mol m^{-3}).

4. Conclusions

The deposited YSZ layer from EPD on the LSM electrode influenced both the transportation of the electrolyte and the electrochemical reaction. However, the contribution of the reduction of reaction rate was more important. In the study, the deposited layer reduced the equilibrium current from −10.47 μA for the blank solution, to −4.17 μA for the suspension. This reduction implied that the deposited YSZ layer would obstruct the electrochemical reaction of the LSM electrode. Although the hydrogen was reduced at the cathode, the proton concentration near cathode unexpectedly increased due to the obstruction of the deposit layer. In the galvanostatic experiments, the retarded reaction rate resulted in the rate-determining step changing from the initially diffusion-controlled reaction, to the reaction-rate-controlled reaction after EPD was performed for a certain time period. As for the potentiostatic experiment, when EPD was performed at −2 to −6 μA, a similar transformation of the rate-determining step changing from a diffusion-controlled reaction to a reaction-rate-controlled reaction occurred with EPD at −2.5 to −12.5 V.

References

[1] H.C. Hamaker, Trans. Faraday Soc. 35 (1940) 186–191.
[2] H.C. Hamaker, E.J.W. Verwey, Trans. Faraday Soc. 35 (1940) 180–185.
[3] E. de Beer, J. Duval, E.A. Meulenkamp, J. Colloid Interface Sci. 222 (2000) 117–124.
[4] H. Koelmans, J.Th.G. Overbeek, Discuss. Faraday Soc. 18 (1954) 52–63.
[5] P. Sarkar, P.S. Nicholson, J. Am. Ceram. Soc. 79 (1996) 1987–2002.
[6] N. Koura, T. Tsukamoto, H. Shoji, T. Hotta, Jpn. J. Appl. Phys. 1 (1995) 1643–1647.
[7] A.J. Bard, L.R. Faulkner, Electrochemical Method, second ed., John Wiley & Sons Inc., USA, 1980, pp 101–109.
[8] P. Zhou, C.W. Wu, G.J. Ma, J. Power Sources 163 (2007) 874–881.
[9] G.H. Guvelioglu, H.G. Stenger, J. Power Sources 163 (2007) 882–891.
[10] K.H. Kwon, C.B. Shin, T.H. Kang, C.S. Kim, J. Power Sources 163 (2006) 151–157.
[11] A. Kusoglu, A.M. Karlsson, M.H. Santare, S. Cleghorn, W.B. Johnson, J. Power Sources 161 (2006) 987–996.
[12] S. Yang, W. Yang, G. Sun, H. Knickle, J. Power Sources 161 (2006) 1412–1419.